



NEW ZEALAND SOCIETY FOR EARTHQUAKE ENGINEERING
**2019 Pacific Conference on
Earthquake Engineering**
TURNING HAZARD AWARENESS INTO RISK MITIGATION
4 – 6 April | SkyCity, Auckland | New Zealand



Development of self-centring Rotational Slip Friction Joint: a novel damage-free damper with large deflections

S. Veismoradi & P. Zarnani

Auckland University of Technology, Auckland.

P. Quenneville

The University of Auckland, Auckland.

ABSTRACT

Rotational friction (RF) dampers are among the efficient energy-absorbing devices with perfectly elasto-plastic behaviour and stable hysteresis response. However, the lack of self-centring features might result in undesirable residual displacement for the buildings equipped with RF dampers, not being reoccupiable quickly after a severe event. This paper introduces an innovative seismic device branded as Rotational Resilient Slip Friction Joint (Rotational-RSFJ) which comprised of especially grooved friction plates clamped by high strength bolts or rods using pre-stressed conical disc springs. Similar to RF dampers, the Rotational-RSFJ provides a remarkable flexibility not only at the connection component design, but also at the structural system performance. In this paper, the principles of force-deflection relationship for the Rotational-RSFJ is analytically developed and validated through finite element analysis. The joint capability for adaptive stiffness and damping is also investigated in principle. Finally, the influence of various parameters affecting the joint performance are analytically analysed as well. As per the findings based on the numerical modelling, it can be deduced that the joint can dissipate the seismic energy through rotational friction sliding while providing a stable and repeatable self-centring feature with no requirement for post-event maintenance, ready for aftershocks.

1 INTRODUCTION

The appropriately designed buildings are expected to provide adequate safety during design level earthquakes without any collapse through introduction of plastic deformations on predefined structural

component such as beam plastic hinges in MRFs, braces in CBFs or weak elements such as sacrificial fuses. While the safety of the occupants is achieved, permanent residual drifts are induced in the structures which are often not easily recoverable after earthquakes and might accumulate during aftershock events and eventually lead to their collapse or demolition (Veismoradi et al. 2018). A study by McCormick et al. (2008) showed that it is rather impractical to repair the damaged structures if the residual drift of the frame exceeds 0.5% given the cost of the repairing could be prohibitively high. Therefore, building owners, design engineers and scholars nowadays seek resilient seismic solutions that could provide minimal residual displacement with negligible damage on the structures, known as low-damage design. To address the residual displacement issue, various structural systems have been developed which utilize self-centring technology. The primary works in the self-centring field were based on adopting post-tensioned steel tendons to introduce the self-centring features on traditional yielding systems (see for example Christopoulos et al. 2002, Christopoulos et al. 2008, Dai et al. 2019, Iqbal et al. 2015, Kurama et al. 1999). As an alternative to cable pre-stressing, some researchers have explored the possibility of utilizing super-elastic shape memory alloys (SMA) to provide the restoring force required for self-centring. A number of studies have investigated the seismic performance of SMAs in various applications and pinpointed the satisfying performance of the SMA-equipped structures with negligible residual drifts, as compared to conventional ones (Alam et al. 2012, Shiravand et al. 2017, Qiu et al. 2017, among many others).

In general, a combination of energy dissipation damper with an elastic spring can present the self-centring flag-shape behaviour which could provide the two key characteristic required to minimise the earthquake damage in structures (i.e. damping and self-centring) (Zarnani et al. 2016). Friction sliding is one the most efficient energy dissipation mechanism among passive devices, offering high level of stiffness and rigid plastic rectangular loops (Mirtaheri et al. 2011), without any damage or plasticisation of the component. This study introduces an innovative seismic device named Rotational Resilient Slip Friction Joint (Rotational-RSFJ) which provides damage-free friction energy dissipation, large deflections and self-centring features, all in one compact device. In this paper, firstly, the joint is investigated at component level and the analytical equations are derived to predict the hysteresis performance of the joint, force vs deflection. Secondly, modelling of the joint is conducted in commercially available SAP2000 software and verified by finite element analysis. Finally, a parametric study is carried out to numerically investigate several factors influencing the performance of the joint.

2 ROTATIONAL RESILIENT SLIP FRICTION JOINT

The schematic view of the Rotational-RSFJ is provided in Figure 1. As can be noted, the joint is similar to rotational friction (RF) damper introduced by Mualla and Belev (2002). A number of studies have investigated the performance of RF-dampers in different bracing systems (see for example Mualla and Belev 2002, Monir and Zeynali, 2013) and base isolation systems (as supplemental damping device) (Nielsen et al. 2004). Figure 2 shows some of the structural applications of the rotational friction damper. The experimental and theoretical results confirm the stable hysteresis of RF dampers over many cycles without any damage to the steel plates. They can also present remarkable flexibility in design, structural application and installation as well. However, the lack of self-centring might indicate the risk of residual displacements for the buildings equipped with RF-dampers in seismically active areas.

The Rotational-RSFJ can solve the self-centring shortcoming of the traditional RF damper while preserving the advantages of RF damper. The Rotational-RSFJ can be designed with various configurations to satisfy the different structural needs and can be easily installed in different structural configuration as well.

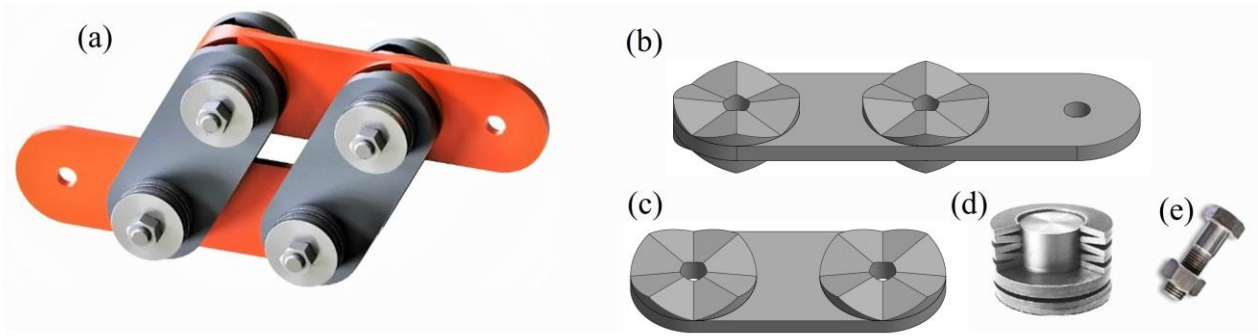


Figure 1: Rotational-RSFJ and its components: (a) schematic view of the damper assembly; (b) middle plate; (c) cap plate; (d) conical disk spring; (e) high strength bolt

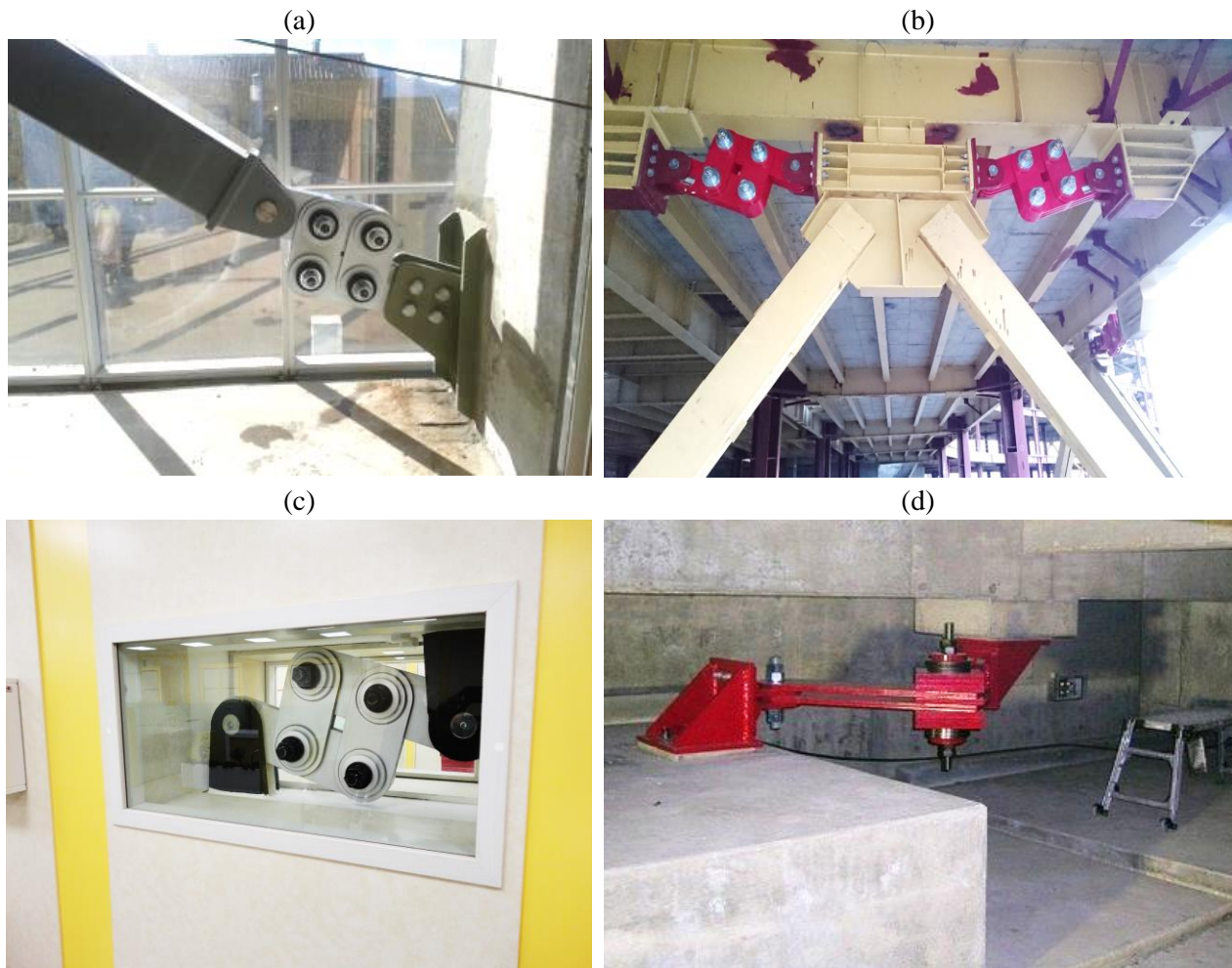


Figure 2: Some of the rotational friction damper applications: (a) diagonal bracing system, (b) V-bracing, (c) panel wall dampers and (d) as a supplemental damping mechanism combined with elastomeric bearing (photos were downloaded from www.dampotech.com)

2.1 Analytical and numerical investigation of friction plates performance

The general concept and performance of the rotational-RSFJ is somewhat similar to RSFJ (Zarnani and Quenneville, 2015) as they both comprise of especially grooved cap and middle plates, clamped by pre-stressed high strength bolt (or rods) and disk springs. Readers can find a thorough review of the RSFJ and its applications in Zarnani et al. (2016), Hashemi et al. (2017a), Hashemi et al. (2017b), and Hashemi et al. (2019).

Paper 114 – Development of self-centring Rotational-RSFJ: a damage-free damper with large deflections

Contrary to RSFJ which dissipates the energy through axial sliding of the plates, the Rotational-RSFJ utilizes rotational friction sliding of its plates to dissipate the seismic energy. Sliding occurs in circular section of the plates, denoted as friction plates. In the Rotational-RSFJ, based on specific force-deflection demand for each design, different deflections and capacities can be achieved by changing the length of the lever arms in cap and middle plates as well as number of the friction plates and angle of the grooves. In addition to the presented symmetric joint in Figure 1-a (with cap plates at both sides of the middle plates), an asymmetric configuration is also possible (with cap plates at only one side of the middle plates only). As the external moment overcomes the friction resistance between the clamped surfaces, the rotational sliding occurs. Using the free body diagram shown on Figure 3 and integrating the overall friction moment provided by each friction plate, the following equations for determining the slip moment (M_{slip}) and the residual moment ($M_{residual}$) of a single symmetric friction plate can be drawn:

$$M_{slip} = \int_{R_{pin}}^{R_{Friction\ Disk}} r dF_{slip} = \int_{R_{pin}}^{R_{Friction\ Disk}} \frac{2F_{bolt.pr}}{R_{Friction\ Disk} - R_{pin}} \left(\frac{L + \mu_s \theta_p r}{\theta_p r - \mu_s L} \right) r dr \quad (1)$$

$$M_{res} = \int_{R_{pin}}^{R_{Friction\ Disk}} r dF_{res} = \int_{R_{pin}}^{R_{Friction\ Disk}} \frac{2F_{bolt.pr}}{R_{Friction\ Disk} - R_{pin}} \left(\frac{L - \mu_k \theta_p r}{\theta_p r + \mu_k L} \right) r dr \quad (2)$$

Where L is the height of the groove, $R_{Friction\ plate}$ is the radius of the friction plate, R_{pin} denotes the radius of the bolt hole and θ_p represent the angle of each surface slice which indicates the maximum theoretical rotation capacity for each friction plate (for example, the friction plates on Figure 1 have eight surface slices with angle of 45 degree). Possible choices for θ_p could be 30°, 45°, 60° or 90° which represents 12, 8, 6 and 4 slices for the whole circular grooved surface, in turn. The parameter μ_s denotes the static coefficient of friction and μ_k is the kinetic coefficient of friction. While previous studies assumed $\mu_k = 0.85\mu_s$ (Hashemi et al. 2017b), by utilizing grease lubrications, the difference between the two friction coefficient could be decreased even more. The maximum bolt force ($F_{b,u}$) can be determined using Equation 3 in which K_s and Δ_s correspond to the total stiffness of the springs stack and their maximum deflection when they are fully flattened at maximum deflection.

$$F_{b,u} = F_{b,pr} + K_s \times \Delta_s \quad (3)$$

The ultimate load upon loading (M_{ult}) and the restoring load upon unloading ($M_{restoring}$) can be calculated by replacing μ_s , μ_k and $F_{bolt,pr}$ with μ_k , μ_s and $F_{bolt,u}$ in Equations 1 and 2, respectively. Figure 4 shows the schematic moment-rotation hysteresis loop for the friction plates.

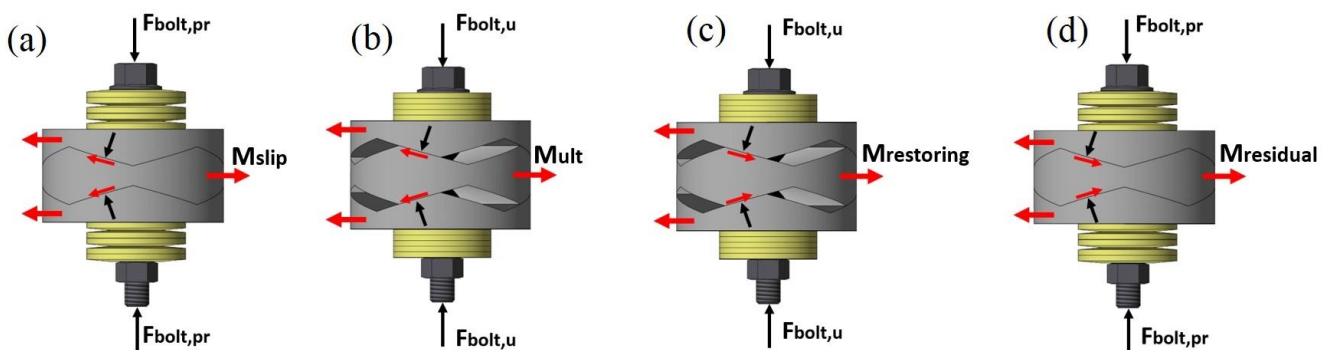


Figure 3: Free body diagram for a symmetric friction plates: (a) at initial slipping; (b) at ultimate loading; (c) at ultimate unloading (restoring); and (d) at restored position

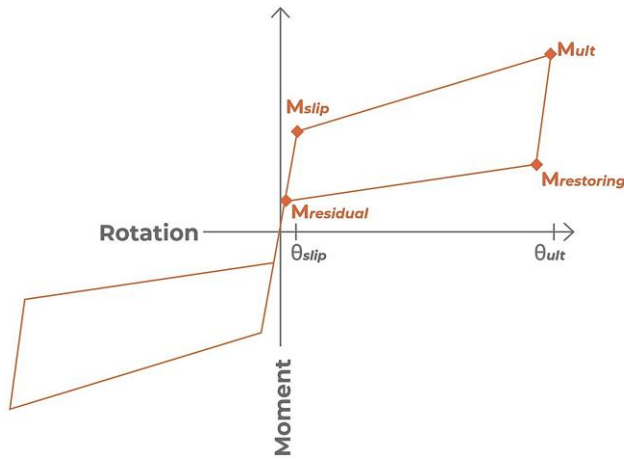


Figure 4: The moment-rotation hysteresis loop for the friction plate

To verify the predictive equations, the finite element model of an asymmetric friction plate was conducted using Abaqus software platform (2012). The friction plates were assumed to have outside groove angle $\theta_{groove}=15^\circ$, with overall diameter of $D_{friction\ plate}=125\text{mm}$ and pin diameter of $D_{pin}=36\text{mm}$. The disk springs were assumed to be pre-stressed at $F_{b,pr}=66\text{kN}$ and provide the ultimate force of $F_{b,ult}=132\text{kN}$, $\Delta_s=7.875\text{mm}$, representing actual stack of nine disk springs placed in series with ultimate capacity of 132kN with internal height of 1.75mm . The slip motion was allowed utilizing a contact element with surface-to-surface discretization. The tangential behaviour of the contact was modelled by penalty method with static and kinetic friction coefficient equal to 0.18 . For the normal direction, the pressure-overclosure feature of the Hard-contact was assumed for the friction model. Figure 5 shows the Von-Mises stress contours of a single asymmetric friction plate and compares the analytical predictions versus the obtained FE results which are in a very good agreement.

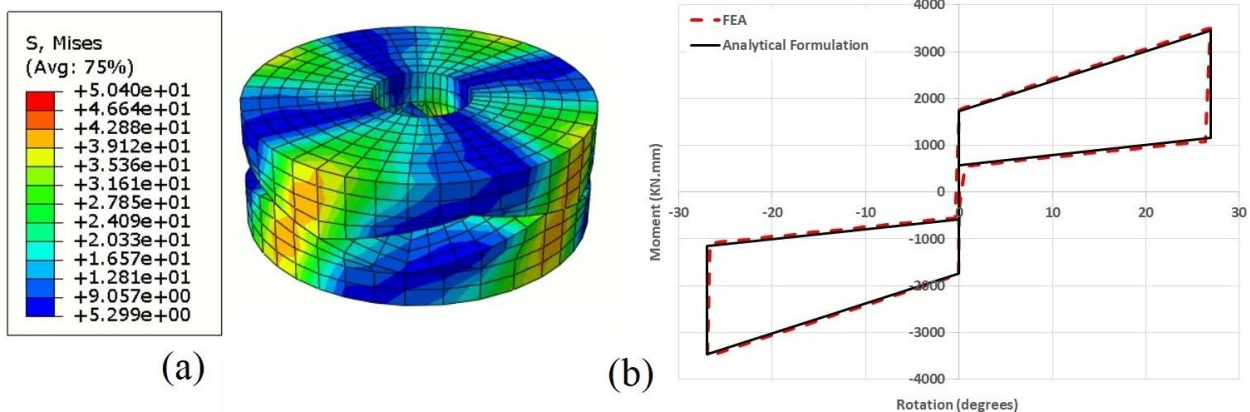


Figure 5: The FEM analysis of a single friction plate: (a) stress distribution; (b) comparison between analytical equations and FEM outcomes

2.2 Joint assembly considerations and modelling – Friction Spring link element

The Rotational-RSFJ comprised of several cap and middle plates, clamped by means of bolts and pre-stressed disk springs. Figure 6-a shows the simplified structural model for the joint assembly. In addition to the radius of friction plates, different length of plates could also be selected ($L1$, $L2$ and $L3$), based on each specific design or deflection requirement. In general, increasing the plate length would provide more deflection capacity with lower force. The effective length of the joint (AB) which is shown on Figure 6-a can be calculated using the following equation:

Paper 114 – Development of self-centring Rotational-RSFJ: a damage-free damper with large deflections

$$AB = \frac{2L_3 + L_2 + L_1 \cos(\beta)}{\cos(\alpha)} \quad (4)$$

Where the parameter α can be obtained by:

$$\alpha = \text{Arctan} \left(\frac{L_1 \sin(\beta)}{2L_3 + L_2 + L_1 \cos(\beta)} \right) \quad (5)$$

The four friction plates act in parallel as they have equal rotation during the joint performance (Chen and Hao 2013). The relation between the joint force and the moment of each friction plate is calculated by Equation 6:

$$F = \frac{4M}{(2L_3 + L_2) \sin(\alpha)} \quad (6)$$

Where M is the frictional moment provided by each friction plate. Based on the correlation between the force of damper and the induced moment of friction plate (Equation 6), and also the overall length of the joint in each angle of friction plate rotation, the force-displacement curve of the joint can be evaluated. The cyclic performance of the friction plates can also be modelled using SAP2000 software package (CSI, 2015). Using the SAP2000, the required thickness of the cap and middle plates can be designed. Table 1 presents a summary of the characteristics for the joint modelled in the SAP2000. The angle $\beta=108^\circ$ was selected to ensure the same amount of deflection for the joint in its open and closed position (ultimate tension and ultimate compression stage). Figure 6-b compares the flag-shaped hysteresis behaviour from theoretical formulations and the one obtained from SAP2000 numerical outcome. For this graph, the $F-\Delta$ has been plotted for four distinctive points (F_{slip} , F_{ult} and associated deflection for 9° and 18° rotation of friction plates in both direction). As can be noted, the post-slip stiffness of the Rotational-RSFJ is variable and slightly changes with further deflection of the joint, due to the second-order geometric effects (the factor $1/\sin(\alpha)$ in Equation 6).

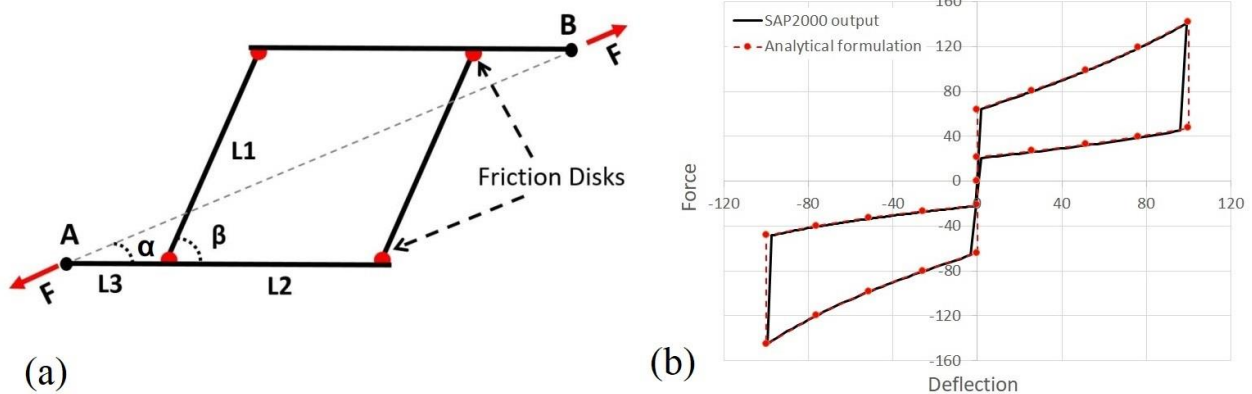


Figure 6: (a) Simplified joint model for implementing in SAP2000 and (b) verification of joint analytical behaviour with SAP2000 numerical results

Table 1: Summary of the joint characteristics

	Parameter	Unit	Value
Joint Characteristics	Cap plate thickness	mm	12
	Middle plate thickness	mm	20
	β	degree	108
	Friction plate diameter	mm	125
	Pin hole diameter	mm	36
	Coefficient of Friction	-	0.18
Disk Spring parameters	Disk spring ultimate force	KN	132
	Disk spring deflection capacity	mm	1.75
	No. of disk spring per bolt per side	-	9
SAP2000 Parameters	Slipping stiffness (loading)	KN.mm/rad	7368.9
	Slipping stiffness (unloading)	KN.mm/rad	2458.1
	Pre-compression displacement (dc)	rad	-0.468
	Stop displacement (ds)	rad	0.47

2.3 Finite Element Analysis of the joint

To verify the analytical equations for the joint assembly and also validate the SAP2000 model, the same joint was modelled in Abaqus FE analysis software. The standard solver was employed for the analysis. The high strength steel ($F_y=690\text{MPa}$ and $F_u=860\text{MPa}$ with 18% elongation) with isotropic hardening behaviour was considered for material modelling. The cap plates and middle plates were modelled using deformable solid parts meshed by C3D8R finite element (an 8-node linear brick with reduced integration). To reduce the solution time needed by the software, only the upper half of the joint was modelled (two cap plates with half of the middle plate). For the contact modelling, both the "Hard contact" normal behaviour (to avoid overclosure) along with tangential behaviour with relative sliding (by assigning Coulomb friction law) was considered with single value of $\mu=0.18$ for both static and kinetic friction coefficients. Instead of modelling the rods and the stack of disk springs, their pre-stressing effects were replicated using spring/dashpot feature of the software. The analysis was performed considering two loading steps: (i) applying the pre-stressing force on the cap plate (to simulate the bolt clamping) and (ii) displacement history application. Figure 7-a depicts the von-Mises stress contour of the joint at nearly 100mm compressive deflection, while Figure 7-b compares the Abaqus numerical outcomes with the analytical formulation presented at previous section. As can be noted, the FE outputs are in a very good agreement with the derived analytical equations.

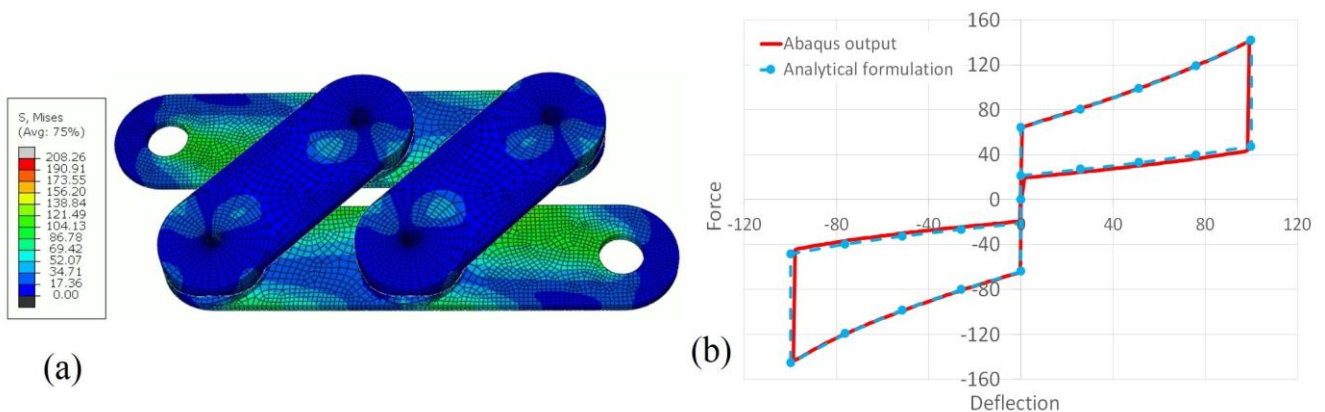


Figure 7: FE analysis of the joint assembly: (a) Von-Mises stress counter at ultimate compression; (b) comparison of the analytical formulation with FE analysis

3 JOINT'S PARAMETER EFFECTS

For this section, some of the influencing parameter affecting the performance of the joints are investigated. Since the performance of the joint is directly related to the friction plates' behaviour, the parametric study is focused on the friction plates, rather than the whole joint assembly. Generally, two main categories affect the joint performance which are parameters related to disk spring arrangement and characteristics related to the friction plates.

As for the disk spring arrangement, different stacks of disk springs can be utilized for providing wide range of force-deflections. Figure 8 shows the different stacking arrangement (parallel, series or combination of both), along with the effect of each arrangement on the performance of the friction plates. While increasing the number of series stacking does not change the M_{slip} and M_{ult} , it increases the rotation capacity of the friction plates. On the other hand, doubling the stack of disks does not change the rotation capacity of the joint, whereas it can double up the M_{slip} and M_{ult} of the friction plate and increase the damping of the system as well. Moreover, parallel stacks of disk springs present some friction between the disk springs' surfaces known as self-dampening. However, it is recommended to lubricate the surfaces of disks in parallel stacks and the maximum number of parallel sets be limited to 4 to reduce the deviation from calculated characteristics of the disk spring stack to the actual measured ones.

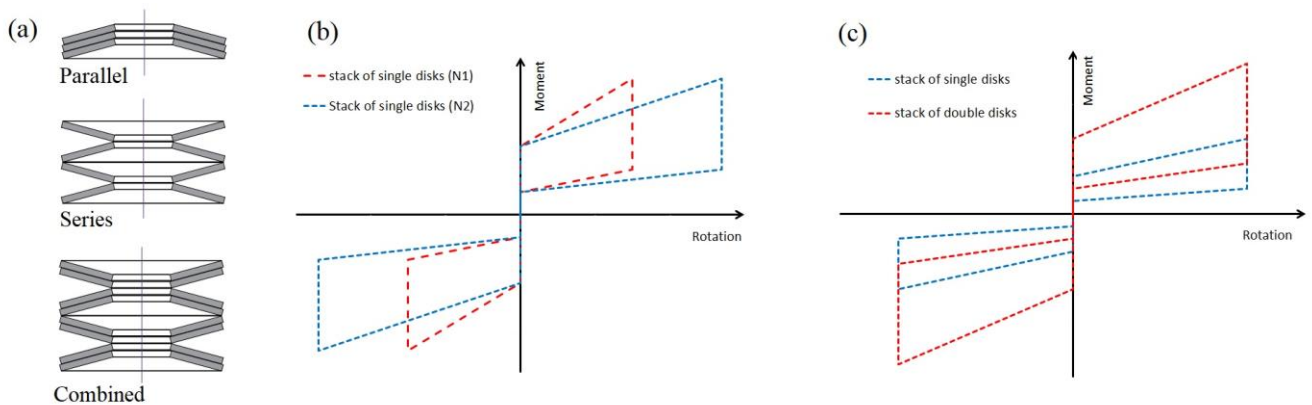


Figure 8: Effect of disk spring arrangement: (a) common practical arrangements; (b) effect of number of washers ($N2 > N1$); (c) Effect of number of parallel stacks (stack of single washers vs. double washers)

While the most prevalent engineering applications usually utilize parallel or series stacking of disk springs, other options such as progressive stacking could also be utilized for the disk spring arrangement of friction plates. On this basis, the disks become flat consecutively and provide a progressively increasing stiffness. This can be achieved by either stacking disks of various thickness in series, or stacking single, double and triple parallel set in series (Figure 9-a). Accordingly, the pre-stressed friction plate demonstrates a progressively increasing multi-linear self-centring flag-shape (Figure 9-b) with distinctive post-slipping stiffness (zones). The single, double and triple parallel set of disk springs would reach their capacity in turn and become flat, as the load increases in the stack of disk springs. When the single parallel set becomes flat, the hysteresis curve surpasses the zone 1 and enters the zone 2 where double and triple parallel sets of disk springs have deflection capacity, while the zone 3 is provided by the remaining deflection capacity of the triple parallel set of disk springs when the single and double parallel sets have reached their ultimate force. Such a progressive self-centring behaviour might be helpful in specific applications and situations where the joint needs to be separately optimized for various seismic intensities at the same time (for example, adaptive shocking absorbers).

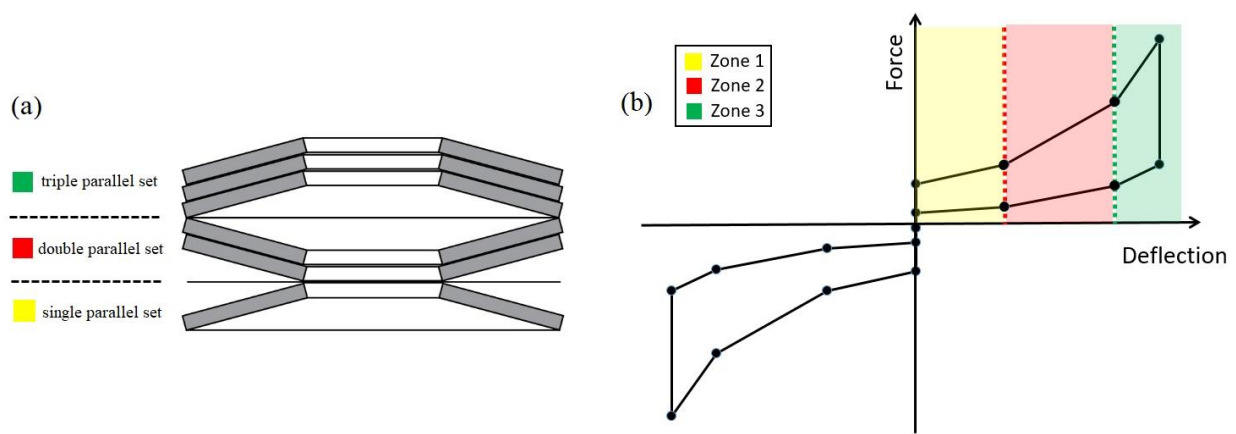


Figure 9: Progressive stacking of disk springs: (a) stack of single, double and triple parallel set in series; (b) The multi-linear self-centring hysteresis behaviour

Regarding characteristics related to the friction plates, the coefficient of friction (COF) and groove angle are investigated. Figure 10 demonstrate the effect of different COFs and groove angles on the $M-\theta$ curve of the friction plates. As can be seen, higher coefficient of friction means higher damping ratios (hysteresis curve) for the joint. On the other hand, higher COFs require larger restoring force to ensure the self-centring of the joint. As for the groove angles, increasing the θ_{groove} would increase the M_{slip} and M_{ult} of the friction plate, with the price of lowering the friction plate rotation capacity. This is due to the increased vertical movement of the cap plate, as a result of larger grooves angle.

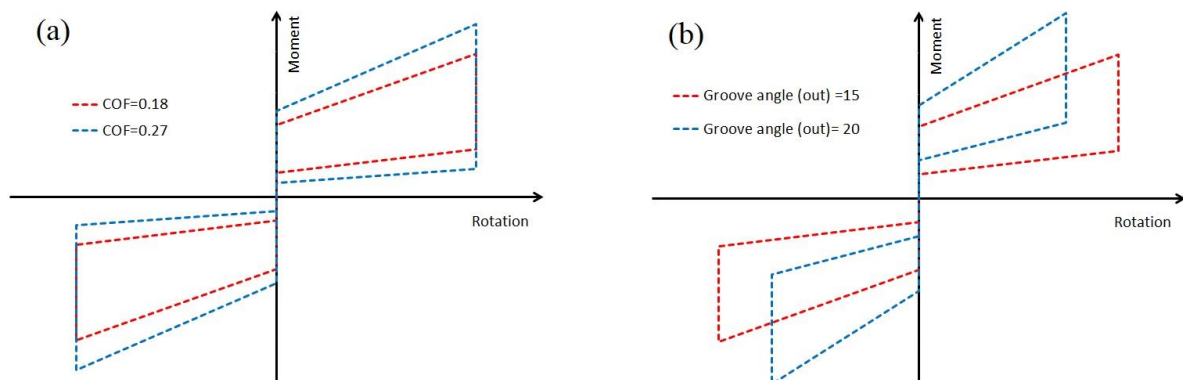


Figure 10: Effect of friction plate characteristics: (a) Coefficient of friction between sliding surfaces; (b) effect of groove angle

4 CONCLUSIONS

In this paper, an innovative self-centring damper branded as Rotational Resilient Slip Friction Joint (Rotational-RSFJ) was introduced and investigated numerically and analytically. This novel damper can be designed based on different force/deformation demands and be utilized in different structural systems as well. The analytical equations for calculating the force-deflection behaviour of the joint was derived and validated using finite element analysis. Moreover, the parameters affecting the joints performance were thoroughly investigated. While the numerical investigations confirm the analytical formulations for this study, experimental testing is planned to be performed in the near future to further validate the performance of the joint. Owing to its remarkable deflection capacity which can be easily modified based on different values of lever arms, the Rotational-RSFJ can also be used in combination with flat-sliding isolation systems in a compact device or as an additional self-centring component connected to the structure at the base level,

to provide the re-centring force for the sliding-isolated buildings. Through this new efficient damper introduced to be used either in new or existing earthquake-prone structures, the buildings could be reoccupied quickly with minimal business interruption and repair costs after severe earthquake events.

5 ACKNOWLEDGEMENTS

The authors would like to thank Ministry of Business, Innovation and Employment of New Zealand (MBIE), for the financial support provided for this research project.

6 REFERENCES

- ABAQUS. 2012. *Analysis user's manual*, Version 6.12.
- Alam, S., Moni, M. & Tesfamariam, S. 2012. Seismic overstrength and ductility of concrete buildings reinforced with superelastic shape memory alloy rebar, *Engineering Structures*, Vol 34 8-20.
- Chen, W. & Hao, H. 2013. Numerical study of blast-resistant sandwich panels with rotational friction dampers, *International journal of Structural Stability and Dynamics*, Vol 13(06), 1350014.
- Christopoulos, C., Filiatrault, A., Uang C.-M. & Folz, B. 2002. Posttensioned energy dissipating connections for moment-resisting steel frames, *Journal of Structural Engineering*, Vol 128(9) 1111-1120.
- Christopoulos, C., Tremblay, R., Kim, H.-J. & Lacerte, M. 2008. Self-centering energy dissipative bracing system for the seismic resistance of structures: development and validation, *Journal of structural engineering*, Vol 134(1) 96-107.
- CSI. 2015. *Analysis reference manual for SAP2000, ETABS, SAFE and CSiBridge*.
- Dai, X.-M., Zong, L., Ding, Y. & Li, Z.-X. 2019. Experimental study on seismic behavior of a novel plug-in self-lock joint for modular steel construction, *Engineering Structures*, Vol 181 143-164.
- Hashemi, A., Yousef-Beik, S.M.M., Darani, F.M., Clifton, G.C., Zarnani, P. & Quenneville, P. 2019. Seismic performance of a damage avoidance self-centring brace with collapse prevention mechanism, *Journal of Constructional Steel Research*, Vol 155 273-285.
- Hashemi, A., Zarnani, P., Masoudnia, R. & Quenneville, P. 2017a. Experimental testing of rocking Cross-Laminated Timber walls with resilient slip friction joints, *Journal of Structural Engineering*, Vol 144(1), 04017180.
- Hashemi, A., Zarnani, P., Masoudnia, R. & Quenneville, P. 2017b. Seismic resistant rocking coupled walls with innovative Resilient Slip Friction (RSF) joints, *Journal of Constructional Steel Research*, Vol 129 215-226.
- Iqbal, A., Pampanin, S., Palermo, A. & Buchanan, A. 2015. Performance and design of LVL walls coupled with UFP dissipaters, *Journal of Earthquake Engineering*, Vol 19(3) 383-409.
- Kurama, Y., Sause, R., Pessiki, S. & Lu, L.-W. 1999. Lateral load behavior and seismic design of unbonded post-tensioned precast concrete walls, *Structural Journal*, Vol 96(4) 622-632.
- McCormick, J., Aburano, H., Ikenaga, M. & Nakashima, M. 2008. Permissible residual deformation levels for building structures considering both safety and human elements, *Proceedings of the 14th world conference on earthquake engineering, Beijing, China*
- Mirtaheri, M., Zandi, A.P., Samadi, S.S. & Samani, H.R. 2011. Numerical and experimental study of hysteretic behavior of cylindrical friction dampers, *Engineering Structures*, Vol 33(12) 3647-3656.
- Monir, H.S. & Zeynali, K. 2013. A modified friction damper for diagonal bracing of structures, *Journal of Constructional Steel Research*, Vol 87 17-30.
- Mualla, I. & Belev, B. 2002. Performance of steel frames with a new friction damper device under earthquake excitation, *Engineering Structures*, Vol 24(3) 365-371.
- Nielsen, L, Mualla, I. & Iwai, Y. 2004. Seismic isolation with a new friction-viscoelastic damping system, *13th World Conference on Earthquake Engineering, Vancouver, Canada*.
- Qiu, C. and Zhu, S. 2017. Performance-based seismic design of self-centering steel frames with SMA-based braces, *Engineering Structures*, Vol 130 67-82.
- Shiravand, M., Nashtae, M. & Veismoradi, S. 2017. Seismic assessment of concrete buildings reinforced with shape memory alloy materials in different stories, *The Structural Design of Tall and Special Buildings*, Vol 26(15), e1384.
- Veismoradi, S., Cheraghi, A. & Darvishan, E. 2018. Probabilistic mainshock-aftershock collapse risk assessment of

buckling restrained braced frames, *Soil Dynamics and Earthquake Engineering*, Vol 115 205-216.

Zarnani, P., Valadbeigi, A. & Quenneville, P. 2016. Resilient slip friction (RSF) joint: A novel connection system for seismic damage avoidance design on timber structures, *World Conf. on Timber Engineering WCTE2016, Vienna, Austria*.

Zarnani, P. & Quenneville, P. 2015. *A resilient slip friction joint*, Patent No. WO2016185432A1, NZ IP Office.